*Acta Cryst.* (1983). A**39**, 719–724

# The Experimental Determination of Phases of Reflections from Mosaic Crystals. 1. $ZnWO_4$*

BY PING PO GONG† AND BEN POST

*Physics Department, Polytechnic Institute of New York, 333 Jay Street, Brooklyn, New York 11201, USA*

(*Received 6 December 1982; accepted 19 April 1983*)

## Abstract

The signs of large numbers of phases of reflections from centrosymmetric crystals of $ZnWO_4$ have been determined by methods outlined by Post [*Acta Cryst.* (1979), A**35**, 17–21; (1983), A**39**, 711–718]. Fifty-three $n$-beam interactions were selected to illustrate the phase determination procedure. Methods of extracting three-beam phase information from such interactions are discussed and illustrated.

## Introduction

A procedure for the experimental determination of the phases of X-ray reflections from single crystals has been described by Post (1979). Examples of successful applications of the method to relatively perfect crystals were given in that publication. In this manuscript we discuss the results obtained when the procedure is applied to mosaic centrosymmetric crystals.

The theoretical basis for the experimental determination of phases is outlined in the preceding paper (Post, 1983). The phases are derived from analyses of the distributions of three- and four-beam intensities about their exact $n$-beam settings. A procedure for generating $n$-beam diffraction systematically was described by Renninger (1937). We use a similar procedure in our work, modified to improve resolution.

In Renninger diffraction a counter detector is used to monitor the intensity diffracted by a set of planes normal to the rotation axis. In the course of the rotation, simultaneous $n$-beam diffraction is generated whenever reciprocal-lattice points (r.l.p.'s) enter or leave the Ewald sphere. While in their diffracting positions, those r.l.p.'s form coupled systems with the two r.l.p.'s, *e.g.* 0 and $H$, which remain in diffracting position on the surface of the sphere. The effects of the interactions on the 'background' intensity, *i.e.* on the otherwise constant two-beam intensity, are analyzed by the methods of dynamical diffraction. The analysis shows that the diffracted intensities are generally displayed in a sequence consisting of a sharp increase followed by an abrupt decrease, or the reverse, depending on whether the invariant phase of the group of reflections involved in the interaction is positive or negative.

## Experimental

$ZnWO_4$ crystallizes in the monoclinic system, space group $P2/c$.‡ There are two formula units in each unit cell: $a = 4{\cdot}691$, $b = 5{\cdot}720$, $c = 4{\cdot}925$ Å and $\beta = 90{\cdot}6°$. A crystal was cleaved to form a square platelet, about 1 × 1 cm and about 1 mm thick. The large face was normal to [010]; it showed some scratches and natural contours. According to Palache, Berman & Frondel (1963), this type of $ZnWO_4$ crystal usually contains small amounts of iron, calcium and manganese, in substitution for zinc.

For $n$-beam diffraction the incident beam should be essentially monochromatic, with small divergence in the beam cross section, preferably no greater than 30″. Crystal-monochromatized beams are usually adequately monochromatic, with satisfactory divergence in one direction, *i.e.* in the plane of incidence. The divergence perpendicular to the plane of incidence is generally too large; to reduce it to permitted levels, a narrow slit may be inserted in the incident beam, near the crystal. In our experiments we have used large source-to-specimen distances to provide monochromatic diffracted beams by separating unwanted radiations from the diffracted Cu $K\alpha_1$ beams. Beam divergence is controlled by placing a small pinhole near the crystal. The divergence is then fairly uniform in all directions, but it must be increased to about 2′ to provide enough intensity. The arrangement is not ideal, but it is simple and inexpensive and has enabled us to collect large amounts of useful $n$-beam diffraction data.

* This work was supported by the National Science Foundation and, in part, by the Joint Services Electronics Program of the US Defense Department.

† Taken, in part, from the Dissertation submitted to the Faculty of the Polytechnic Institute of New York in partial fulfilment of the requirements for the degree Doctor of Philosophy (Physics), 1982.

‡ The authors are indebted to Dr William Roth, of the National Bureau of Standards, for providing the $ZnWO_4$ and other crystals used in this research.

0108-7673/83/050719-06$01.50

In Fig. 1 we show a schematic diagram of our experimental arrangement. The radiation source is a Philips X-ray generator equipped with a fine-focus copper-target tube. At a 4° take-off angle, the effective size of the focal spot is about 400 × 500 μm. A 120 cm long evacuated tube between the source and the specimen reduced losses due to absorption by air as well as background radiation near the direct beam. A 0·5 mm pinhole near the crystal reduced incident-beam divergence to less than 2′. The crystal was rotated about a horizontal axis at about 0·5° $min^{-1}$ to record $n$-beam patterns.

Procedures for the calculation of the azimuthal angles at which $n$-beam interactions occur have been outlined by Cole, Chambers & Dunn (1962) and by Post (1975). They are used to identify the reflections involved in each interaction and, in some instances, to refine crystal lattice constants.

The crystal was aligned carefully to bring the [040] diffraction vector into coincidence with the goniometer rotation axis. The alignment was considered satisfactory when the maximum variation of the two-beam intensity in a 360° scan was less than three or four times the expected error due to counting statistics. Crystal alignment techniques are discussed by Post (1975).

As the crystal is rotated, each accessible r.l.p. enters the Ewald sphere at an azimuthal angle $\varphi_i$ and emerges at $(\varphi_i + 2\beta_i)°$. The rotation axis, [040] in the case considered, has twofold rotational symmetry. Each pair of interactions was therefore displayed twice in our 360° scans, once with the 'normal' intensity sequence, and once with the sequence reversed. These provide useful multiple checks on the validity of the indexing procedures.

## Experimental results and discussion

### (*A*) *Four-beam diffraction: general*

The use of the $b$ axis of a monoclinic crystal as the rotation axis in a Renninger-type experiment, such as the one dealt with in this manuscript, favors the generation of four-beam diffraction. R.l.p. ($hkl$) enters and leaves the Ewald sphere simultaneously with r.l.p. ($hk'l$), where $k'$ equals $K$(rotation) − $k$. Systematic three-beam diffraction then occurs when, and only when, the $k$ index of the secondary reflection equals $K$(rotation)/2.

In four-beam diffraction, the four relevant r.l.p.'s are usually located at the corners of a rectangle or a trapezoid in reciprocal space. The crystal rotation axis is then parallel to a side of the rectangle or to the sides of the trapezoid which are parallel to one another (Fig. 2).

An interesting feature of four-beam simultaneous diffraction has been discussed briefly by Post, Chang & Huang (1977), in a publication dealing with four-beam interactions in germanium. The four r.l.p.'s (000), (1$\bar{1}$1), (220), (311) are situated at the corners of a rectangle. When the rotation axis corresponded to a side of the rectangle, the calculated and experimental distributions of diffracted intensities showed significant asymmetries along the two-beam line. For the same set of r.l.p.'s, the intensity asymmetries vanished when a diagonal of the rectangle served as the rotation axis. These effects are illustrated in their Figs. 3, 6, 7, 8.

The intensity asymmetries were attributed to the simultaneous entry into the Ewald sphere of two equivalent r.l.p.'s. In the case considered both r.l.p.'s were located on the same side of the rectangle, parallel to the rotation axis. The symmetric case (rotation about a diagonal) also involved two r.l.p.'s passing simultaneously through the surface of the Ewald sphere, but in opposite directions.

It is evident that the diffraction effects which characterize entry of a r.l.p. into the Ewald sphere must be reversed in sequence when that r.l.p., or a symmetry-related one, emerges from the sphere. In such cases, the superposition of the two effects destroys the intensity asymmetry which is generated when both move in the same direction. In both the symmetric and the asymmetric cases, intensity enhancement may be observed very close to the exact three-beam line. Only the

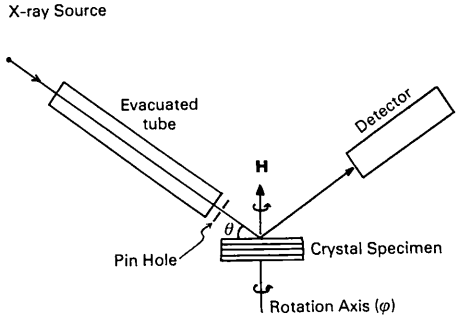


Fig. 1. Experimental arrangement.

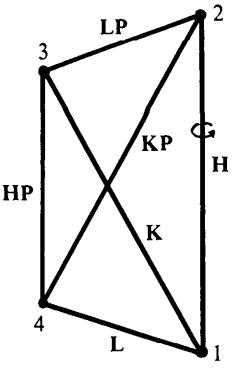


Fig. 2. Arrangement of reciprocal-lattice points in four-beam diffraction. Rotation about **H**.

intensity asymmetry to the right and left of that line is cancelled out.

More complicated situations are encountered in less-symmetrical cases. When four r.l.p.'s are located at the corners of a trapezoid, the magnitudes as well as the phases of the off-diagonal r.l.p.'s will generally differ. In such cases, if the 'entering' and 'emerging' r.l.p.'s have the same phase, their contributions will cancel one another to an extent dependent on the difference between their magnitudes. The effects produced when their phases differ can be readily visualized.

### (*B*) *Four-beam dispersion surfaces*

The calculation of four-beam dispersion surfaces is illustrated for two types of rotation axes in Post, Chang & Huang (1977). That indicates that the dispersion surface which corresponds to the asymmetric case, *i.e.* in which both secondary r.l.p.'s enter the Ewald sphere simultaneously, is of the type depicted in our Fig. 3(*a*).

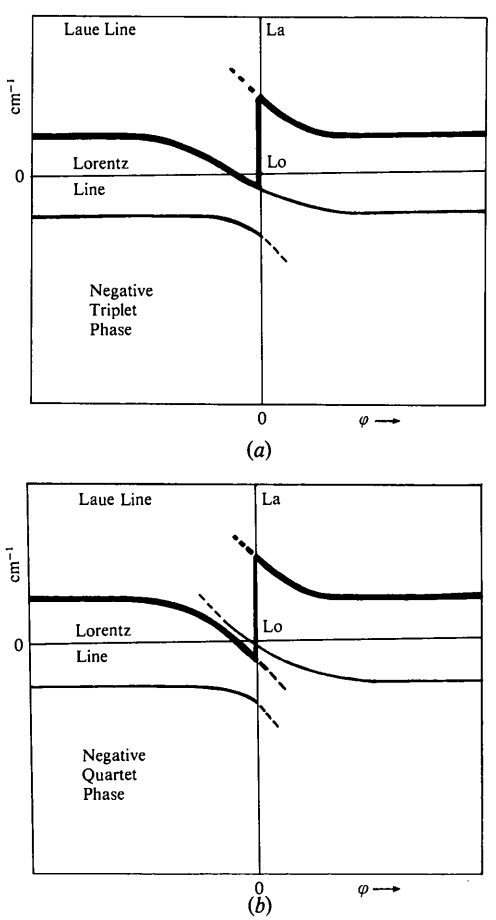


Fig. 3. (*a*) Four-beam dispersion curves; (*b*) three-beam dispersion curves.

To one side of the four-beam setting, near $\varphi = 0$, both branches of the two-beam line curve upward toward the Laue line. On the other side of $\varphi = 0$ both branches curve in the opposite direction, away from the Laue line. The similarity between Fig. 3(*a*) and the corresponding three-beam dispersion surface, shown in Fig. 3(*b*), increases when the effects of absorption are taken into account. It is well known that in real crystals diffraction effects which originate at tiepoints on sheets with large absorption coefficients are absorbed preferentially and usually have little effect on the observed intensities. The sheets involved are those which are furthest removed from the Laue line. The sheet or sheets nearest the Laue line are therefore usually responsible for most of the observed intensities. They are shown as thick lines in Fig. 3.

### (*C*) *A phase relationship in P2/c*

Reflection *H* (Fig. 2) is involved in two triplets: **H**, **K**, **LP** and **H**, **L**, and **KP**. These correspond to the two triangles in the figure with r.l.p.'s 1, 2, 3 and 1, 2, 4 at their corners. In *P*2/*c*, $F(HKl) = F(HK\bar{l})$ for '*l*' even, and $F(HKl) = -F(HK\bar{l})$ for '*l*' odd. It follows that, for *P*2/*c*, the signs of the two reflection triplets are the same for all values of '*l*'.

### (*D*) *Triplet phases from four-beam interactions*

Seven structure-factor invariants may be involved in four-beam interactions. These include four triplets and three quartets. Vectors **H** and **HP** are involved in two different triplets. Both are involved in two of the quartets and neither is present in the third (see Fig. 2). In Fig. 2, the numbers at the corners represent r.l.p.'s; the letters represent reflecting planes. Each closed polygon represents an invariant.

The similarity between the three- and four-beam dispersion surfaces, noted above, suggests the possibility that the variations of two-beam intensities near the exact four-beam setting may be due mainly to the two triplets in which reflection is involved.

In this investigation and in others which involved the determination of phases in lead molybdate and sulfamic acid, it was found that phases based on the above assumption agree, in all instances, with those calculated from known atomic coordinates. More than 200 four-beam interactions, covering wide ranges of intensities, were included in those determinations.

The above is physically reasonable. **HP**, unlike **H**, can diffract only in the brief intervals when r.l.p.'s 3 and 4 are simultaneously in their diffracting positions. All seven invariants may then participate in the diffraction processes. Under these conditions, the experimental determination of meaningful phase signs becomes very difficult. In our work, however, we have always focused on variations of two-beam intensities at

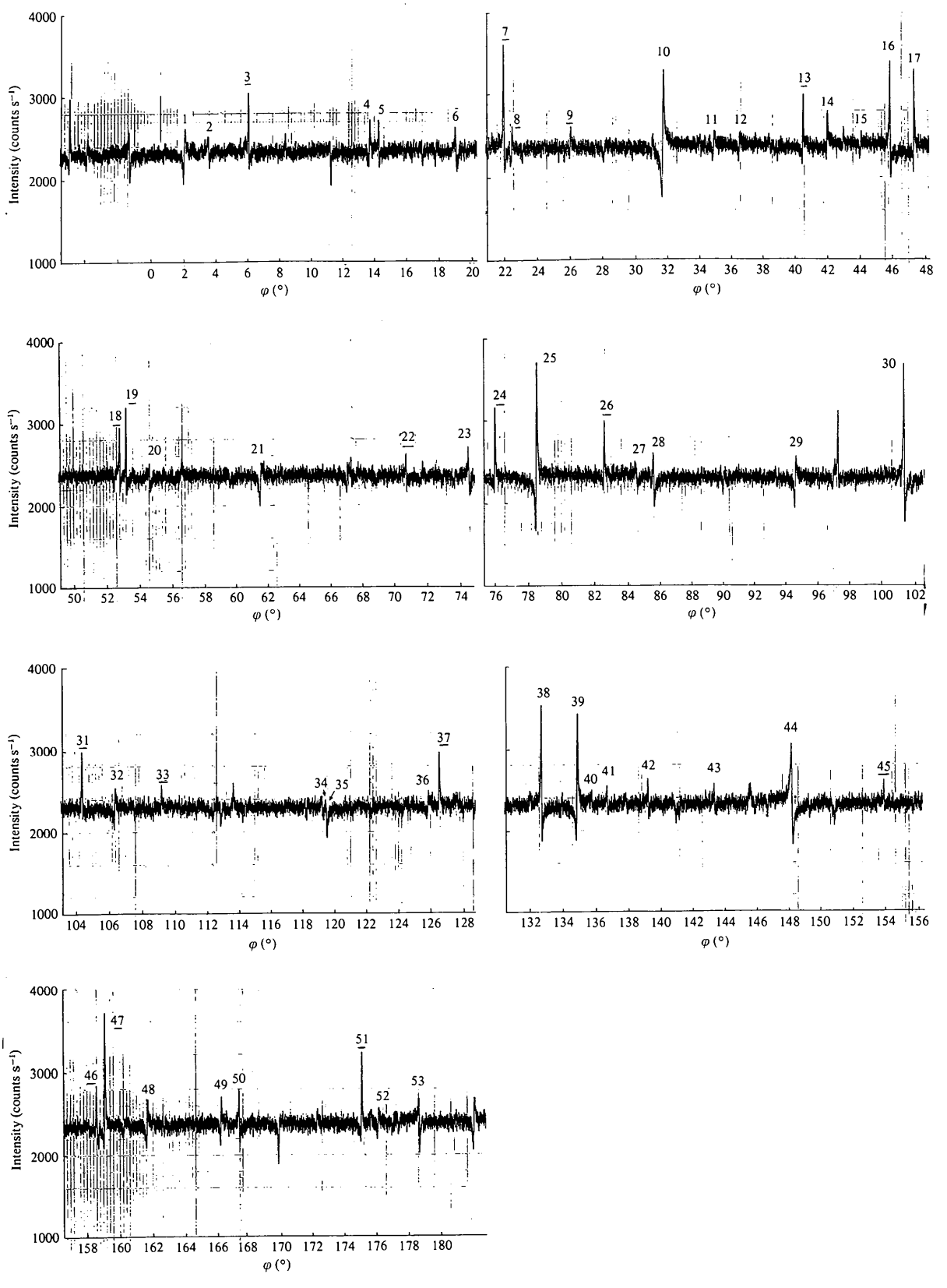


Fig. 4. *n*-Beam diffraction pattern of $ZnWO_4$. Rotation axis: [040]; Cu $K\alpha_1$ radiation.

settings slightly removed from the exact *n*-beam setting. The criteria for four-beam diffraction are clearly more selective than those for three-beam diffraction. **H** participates in three-beam diffraction when either r.l.p. 3 or 4 is excited; the excitation of **HP** requires that both 3 and 4 be excited.

Two of the three quartets involved in the four-beam interaction also involve **HP**. If the contributions of the latter are ignored, only two reflection triplets and one quartet (**K, LP, KP, L**) need be considered in evaluating the diffracted intensities. The quartet could be used to determine the phase of the interaction when both **H** and **HP** have structure factors equal to zero.

### (*E*) *Triplet phase determination*

In Fig. 4 we show a 180° portion of a [040] *n*-beam diffraction pattern of $ZnWO_4$, recorded with Cu $K\alpha_1$ radiation. Fifty-three of the interactions were considered to be sufficiently strong and free from overlap effects to be used to illustrate the phase-determination procedure which we have used. Of these, only 17 involve three-beam interactions. These are indicated by underlining the identifying numbers listed in columns 1 and 3 of Table 1. The latter is a compilation of relevant data for all 53 interactions. Explanations of the table headings are given at the end of the table.

Table 1 provides a useful guide to practical aspects of the phase determination process. In column 3 we list the identifying numbers of interactions related to those whose azimuthal angles are listed in column 1. The relations involve the relative directions of movement through the surface of the Ewald sphere. Where column 1 lists an 'entering' reflection, the corresponding 'emerging' one is listed in column 3, *etc.*

Columns 5 and 6 are most important. The results of the phase determination process are summarized there. In comparing the experimental phases listed in column 5 with the calculated ones in column 6, it should be noted that the symbols $R\uparrow$ and $L\uparrow$ are equivalent to $L$ and $R$, respectively.

The phases in column 5 are assembled in one of two

Table 1. *n-Beam diffraction data for* $ZnWO_4$ (*based on Fig.* 4)

| Identification No.† | $\varphi_i$ (°)‡ | Symmetry related reflection§ | *hkl*/*h'k'l'*¶ | *R*/*L*** | Phase†† | Identification No.† | $\varphi_i$ (°)‡ | Symmetry related reflection§ | *hkl*/*h'k'l'*¶ | *R*/*L*** | Phase†† |
|---|---|---|---|---|---|---|---|---|---|---|---|
| 1 | 3·65 | * | $\bar{1}\bar{1}1/15\bar{1}$ | *L* | + | 28 | 85·65 | 1 | $\bar{1}\bar{1}1/15\bar{1}$ | *R*↑ | + |
| 2 | 3·65 | * | $\bar{3}\bar{1}2/35\bar{2}$ | *R* | − | 29 | 94·65 | 53 | $1\bar{1}1/\bar{1}5\bar{1}$ | *L* | + |
| 3 | 6·15 | 51 | $022/02\bar{2}$ | *R* | − | 30 | 101·40 | 25 | $\bar{1}30/\underline{110}$ | *R*↑ | + |
| 4 | 13·70 | 50 | $01\bar{1}/031$ | *L*↑ | − | 31 | 104·45 | 37 | $\bar{2}21/2\underline{1\bar{1}}$ | *R*↑ | + |
| 5 | 14·40 | 14 | $\bar{1}1\bar{2}/\underline{132}$ | *R*↑ | + | 32 | 106·45 | 6 | $\bar{1}\bar{1}2/15\bar{2}$ | *L*↑ | − |
| 6 | 19·15 | 32 | $\bar{1}\bar{1}2/15\bar{2}$ | *R* | − | 33 | 109·25 | 22 | $\bar{1}20/\underline{120}$ | *L*↑ | − |
| 7 | 22·05 | 47 | $02\bar{1}/021$ | *R*↑ | + | 34 | 119·30 | 52 | $352/\bar{3}1\bar{2}$ | *R* | − |
| 8 | 22·60 | 46 | $023/02\bar{3}$ | *L* | + | 35 | 119·65 | 21 | $051/0\underline{1\bar{1}}$ | *R*↑ | + |
| 9 | 26·08 | * | $\bar{2}2\bar{2}/222$ | *L*↑ | − | 36 | 125·90 | 27 | $1\bar{1}4/\bar{1}5\bar{4}$ | *L*↑ | − |
| 10 | 31·75 | 44 | $\bar{1}50/1\underline{\bar{1}0}$ | *L*↑ | − | 37 | 126·60 | 31 | $22\bar{1}/\bar{2}21$ | *L* | + |
| 11 | 34·90 | * | $\bar{1}53/1\bar{1}\bar{3}$ | *L* | + | 38 | 132·80 | 39 | $13\bar{1}/\bar{1}11$ | *R* | − |
| 12 | 36·58 | 43 | $\bar{3}\bar{1}0/\underline{350}$ | *L*↑ | − | 39 | 134·95 | 38 | $\bar{1}31/11\underline{\bar{1}}$ | *L*↑ | − |
| 13 | 40·55 | 18 | $121/\underline{12\bar{1}}$ | *L* | + | 40 | 135·80 | 15 | $250/\bar{2}\underline{\bar{1}0}$ | *R* | − |
| 14 | 42·05 | 5 | $112/\bar{1}3\bar{2}$ | *L* | + | 41 | 136·73 | * | $33\bar{1}/\bar{3}11$ | *R* | − |
| 15 | 44·10 | 40 | $\bar{2}50/2\underline{\bar{1}0}$ | *L*↑ | − | 42 | 139·25 | 49 | $\bar{1}32/1\underline{1\bar{2}}$ | *R*↑ | + |
| 16 | 45·98 | 17 | $111/\underline{\bar{1}3\bar{1}}$ | *R* | − | 43 | 143·40 | 12 | $3\bar{1}0/\bar{3}\underline{50}$ | *R* | − |
| 17 | 47·45 | 16 | $\bar{1}1\bar{1}/\underline{131}$ | *L*↑ | − | 44 | 148·25 | 10 | $150/\bar{1}\underline{\bar{1}0}$ | *R* | − |
| 18 | 52·85 | 13 | $\bar{1}2\bar{1}/\underline{121}$ | *R*↑ | + | 45 | 154·00 | * | $22\bar{2}/\bar{2}\underline{22}$ | *R* | − |
| 19 | 53·30 | 24 | $2\bar{2}1/\underline{221}$ | *R*↑ | + | 46 | 158·65 | 8 | $023/02\underline{\bar{3}}$ | *R*↑ | + |
| 20 | 54·68 | * | $\bar{1}54/1\underline{1\bar{4}}$ | *R* | − | 47 | 159·15 | 7 | $02\bar{1}/0\underline{21}$ | *L* | + |
| 21 | 61·50 | 35 | $051/0\underline{\bar{1}\bar{1}}$ | *L* | + | 48 | 161·75 | 23 | $152/\bar{1}\underline{1\bar{2}}$ | *L*↑ | − |
| 22 | 70·80 | 33 | $120/\underline{\bar{1}20}$ | *R* | − | 49 | 166·25 | 42 | $13\bar{2}/\bar{1}\underline{12}$ | *L* | + |
| 23 | 74·65 | 48 | $152/\bar{1}\underline{1\bar{2}}$ | *R* | − | 50 | 167·45 | 4 | $01\bar{1}/0\underline{31}$ | *R* | − |
| 24 | 76·10 | 19 | $221/\bar{2}\underline{2\bar{1}}$ | *L* | + | 51 | 175·10 | 3 | $022/02\underline{\bar{2}}$ | *L*↑ | − |
| 25 | 78·60 | 30 | $130/\bar{1}\underline{10}$ | *L* | + | 52 | 176·10 | 34 | $352/\bar{3}\underline{1\bar{2}}$ | *L*↑ | − |
| 26 | 82·65 | * | $\bar{2}20/220$ | *L*↑ | − | 53 | 178·70 | 29 | $1\bar{1}1/\bar{1}\underline{5\bar{1}}$ | *R*↑ | + |
| 27 | 84·55 | 36 | $1\bar{1}4/\bar{1}\underline{5\bar{4}}$ | *R* | − | | | | | | |

† Underlined identification numbers refer to three-beam cases.

‡ $\varphi_i$ refers to the azimuthal angle at which the interaction occurs.

§ Each interaction may appear twice within each 180° range of chart angles, once when it enters the Ewald sphere and again when it leaves. Such related pairs of interactions appear on the same row in columns 1 and 3. Asterisks refer to overlapping interactions.

¶ The *hkl* indices of one secondary reflection and one coupling term are listed for each three- or four-beam interaction. Two pairs of secondary and coupling terms are involved in four-beam interactions; the indices of the second pair may be calculated from the first.

** *R* and *L* refer to the relative locations of the intensity minimum and maximum of each interaction. If the former is to the right of the maximum, an *R* is indicated. The vertical arrow indicates that the interaction, whose azimuth angle is listed in column 1, is emerging from the Ewald sphere. It should be clear that $L\uparrow$ is equivalent to *R*, and $R\uparrow$ to *L*.

†† The listed signs are those of phases calculated from known atomic coordinates.

categories, $R$ or $L$. It is then necessary to establish which category represents the positive and which the negative phase. This can be done conveniently by considering the averages of the magnitudes of the structure factors in each group. We have arbitrarily utilized the product of the magnitudes of the secondary and coupling terms of each interaction as representative of the magnitude of the $n$-beam interaction in which they are involved. The products were normalized by setting the value of the largest one to 100. On that scale, the average product equalled 61 for category $L$ and 21 for $R$. Clearly, the former represented the positive phases. This conclusion was supported by the fact that the largest product in the 'negative' group had a normalized value of only 43.

One minor, but possibly confusing, point should be noted. On most chart recordings, the relative locations of maxima and minima will appear in a sequence opposite to that of the calculated ones. The effect is illustrated in Fig. 5.

We summarize by noting that there can be little doubt that the phases of reflection triplets can be determined directly from the analysis of $n$-beam intensities, for centrosymmetric crystals with relatively small unit cells. The extent to which the procedures outlined above can be used, after suitable modification, to determine phases routinely and correctly for non-centrosymmetric crystals and for crystals with large unit cells remains to be established.

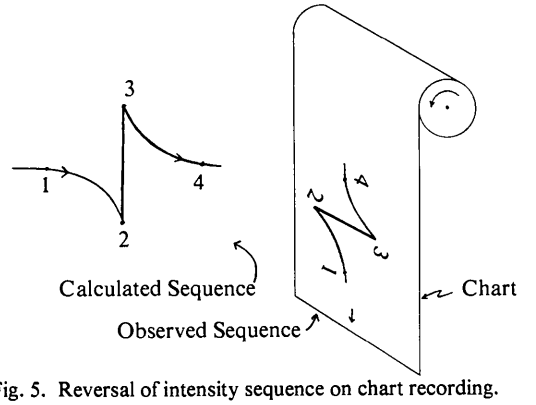


Fig. 5. Reversal of intensity sequence on chart recording.

**References**

COLE, H., CHAMBERS, F. W. & DUNN, H. M. (1962). *Acta Cryst.* **15**, 138–144.
PALACHE, C., BERMAN, H. & FRONDEL, C. (1963). *The System of Mineralogy*, Vol. II. New York: Wiley.
POST, B. (1975). *J. Appl. Cryst.* **8**, 452–456.
POST, B. (1979). *Acta Cryst.* A**35**, 17–21.
POST, B. (1983). *Acta Cryst.* A**39**, 711–718.
POST, B., CHANG, S. L. & HUANG, T. C. (1977). *Acta Cryst.* A**33**, 90–97.
RENNINGER, M. (1937). *Z. Phys.* **106**, 141–176.

*Acta Cryst.* (1983). A**39**, 724–736

# Graphical Enumeration of Polyhedral Clusters

BY F. C. HAWTHORNE

*Department of Earth Sciences, University of Manitoba, Winnipeg, Manitoba, Canada R3T 2N2*

(*Received* 31 *December* 1982; *accepted* 14 *April* 1983)

**Abstract**

The following hypothesis is proposed: *crystal structures may be ordered or classified according to the polymerization of those coordination polyhedra (not necessarily of the same type) with the higher bond valences.* The linkage of polyhedra to form clusters is considered from a graph-theoretic viewpoint. Polyhedra are represented by the chromatic vertices of a (labelled) graph, in which different colours indicate coordination polyhedra of different type. The linking together of polyhedra is denoted by the presence of an edge or edges between vertices representing linked polyhedra, the number of edges between two vertices corresponding to the number of corners (atoms) common to both polyhedra. Information on geometrical isomerism is lost in this graphical representation, but the graphical characteristics are retained. The graph may be completely represented by its adjacency matrix, an $n \times n$ matrix [with $\binom{n}{2} = N$ independent elements] denoting vertex linkage; it is convenient to represent the $N$ independent matrix elements by the ordered set $\{a,b,c,\ldots,N\}$. The collection of all permutations of the vertex labellings that preserve isomorphism is called the automorphism group $\Gamma(G)$ of the graph. $\Gamma(G)$ is a subgroup of the symmetric group $S_n$, and the complementary disjoint subgroup of $S_n$ defines all distinct graphs whose vertex sets correspond to the (unordered) set $\{a,b,c,\ldots,N\}$. However, it is more convenient in practice to work with the corresponding matrix-element symmetries that form

0108-7673/83/050724-13$01.50 